



## Autonomous docking based on infrared system for electric vehicle charging in urban areas

Joshué Pérez Rastelli, Fawzi Nashashibi, Benjamin Lefaudoux, Paulo Resende,  
Evangeline Pollard

### ► To cite this version:

Joshué Pérez Rastelli, Fawzi Nashashibi, Benjamin Lefaudoux, Paulo Resende, Evangeline Pollard.  
Autonomous docking based on infrared system for electric vehicle charging in urban areas. Sensors, 2013. hal-00913122

HAL Id: hal-00913122

<https://inria.hal.science/hal-00913122>

Submitted on 3 Dec 2013

**HAL** is a multi-disciplinary open access archive for the deposit and dissemination of scientific research documents, whether they are published or not. The documents may come from teaching and research institutions in France or abroad, or from public or private research centers.

L'archive ouverte pluridisciplinaire **HAL**, est destinée au dépôt et à la diffusion de documents scientifiques de niveau recherche, publiés ou non, émanant des établissements d'enseignement et de recherche français ou étrangers, des laboratoires publics ou privés.

Article

# Autonomous docking based on infrared system for electric vehicle charging in urban areas

**Joshué Pérez<sup>1,\*</sup>, Fawzi Nashashibi<sup>1</sup>, Benjamin Lefaudoux<sup>1</sup>, Paulo Resende<sup>1</sup> and Evangeline Pollard<sup>1</sup>**

<sup>1</sup> IMARA team at INRIA research center, Domaine de Voluceau-Rocquencourt, BP 105, 78153, Le Chesnay. France.

E-Mails: joshue.perez\_rastelli, fawzi.nashashibi@inria.fr, benjamin.lefaudeux@inria.fr, paulo.lopes\_resende@inria.fr, evangeline.pollard@inria.fr

\* Author to whom correspondence should be addressed; joshue.perez\_rastelli, Tel.: +33139635029.

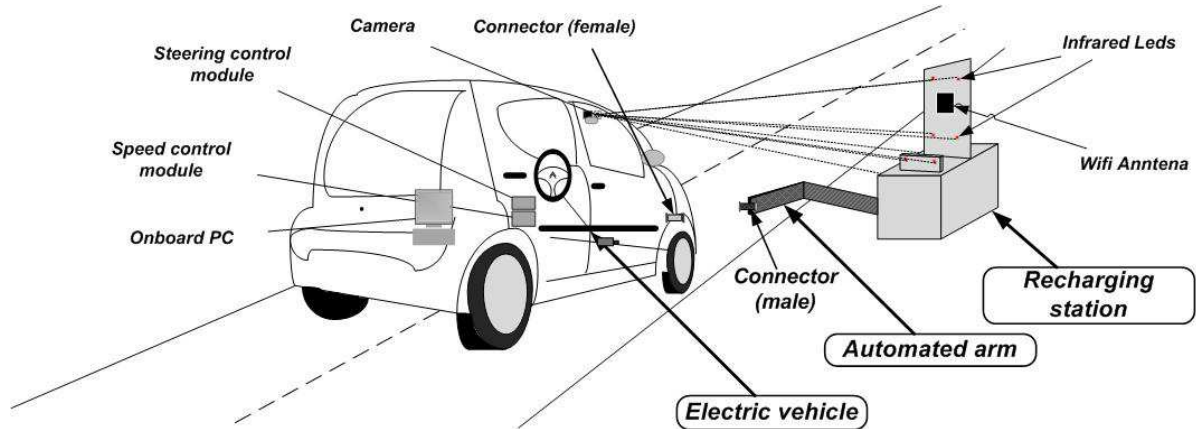
Version January 23, 2013 submitted to Sensors. Typeset by *LATEX* using class file *mdpi.cls*

1       **Abstract:** Electric vehicles are progressively introduced in urban areas because of their  
2       ability to reduce air pollution, fuel consumption and noise nuisance. Nowadays, some big  
3       cities are launching first electric car-sharing projects to clear traffic jams and enhance urban  
4       mobility, as an alternative of the classic public transportation systems. However, there are  
5       still some problems to be solved related to energy storage, electric charging and autonomy.  
6       In this paper, we present an autonomous docking system for electric vehicles recharging  
7       based on an embarked infrared camera performing infrared beacons detection installed in  
8       the infrastructure. A visual servoing system coupled with an automatic controller allow the  
9       vehicle to dock accurately to the recharging booth in a street parking area. The results show  
10      a good behavior of the implemented system, which is currently deployed as a real prototype  
11      system in the city of Paris.

12      **Keywords:** Autonomous parking; Electric vehicle; Vision systems; Docking system; Lateral  
13      control

## 14      1. Introduction

15      Today, a wide variety of Advanced Driver Assistance Systems (ADAS) are available in conventional  
16      vehicles. These systems allow multiple improvements in driving assistance and some partial control such  
17      as: blind angle detection systems [1], lane departure warning [2], speed limit warning [3], pedestrian

**Figure 1.** Elements of the system and docking maneuver of the AMARE project

18 collision avoidance [4], parking assistance [5] (among others). Nevertheless, some other ITS topics  
 19 are improved for research groups around the world. The European Union, specifically the Directorate-  
 20 General for Mobility and Transport of the European Commission (EC), develops transport policies by  
 21 integrating citizen needs, environmental policy, and competitiveness [6].

22 One of the main objectives of the EC is to decrease the use of gas-propelled vehicles in 2050, reducing  
 23 transport sector emissions of greenhouse gas (GHG) by about 60%. Therefore, electric vehicles (EV)  
 24 will improve the urban transportation because of their efficiency and the absence of CO<sub>2</sub> gas emissions  
 25 and noise. In fact, some fully automated electric vehicles are already in use in airports, private tracks  
 26 and pedestrian zones in urban areas [7,8]. However, the market penetration of EV depends on the  
 27 improvement of the electric vehicle batteries, in terms of battery costs, operational autonomy and the  
 28 distribution of charging points availability in the cities.

29 With the growth of EV industry more charging points will appear at motorway service stations and in  
 30 major cities. This year, in the United States, there are more than eight thousand public charging stations  
 31 [9]. However, there are still some lacks in this solution due to the slow charging times and the parking  
 32 problems. Some authors have applied Inductive Power Transfer (IPT) techniques for EV recharging  
 33 [10]. Although this system offers a safe, convenient and reliable solution, its implementation depends  
 34 on the performance of the power pads, and this technology is unavailable for all types of EV's. Other  
 35 works are focusing on the fast-charging electric issues, performing simulations of a recharging station  
 36 with different platforms [11]. These first results suggest a quick implementation of charging stations for  
 37 EVs in urban and inter-urban scenarios.

38 In the last years, autonomous vehicles, chiefly using EV, have been gradually improved in terms  
 39 of safety and redundancy. Cyberscars are a good example of this evolution, since they allow fully  
 40 autonomous driving capabilities for specific scenarios in order to provide an on-demand door-to-door  
 41 service [7]. These vehicles use a GPS sensor for positioning, and wireless communications for  
 42 interaction with other vehicles and the infrastructure [12]. IMARA group of INRIA (National Institute  
 43 for Research in Computer Science and Control, France) is working in the development of perception and  
 44 control strategies for Cyberscars[8,13].

45 Other works propose the control of autonomous EV with mathematical modelling of the motion  
 46 dynamics and drivability control to optimize the operating freedom of two power trains in hybrid electric

47 vehicle [14]. In [15], a real vehicle modified with a steer-by-wire system and Global Positioning System  
48 (GPS) for localization is proposed. Moreover, Intelligent Artificial (IA) techniques, such as fuzzy logic  
49 [12] and Neural-Networks (NN) [16], have been used to control real vehicles in urban and highway  
50 scenarios, based on human experiences and cooperative GPS and inertial systems [17].

51 About the localization problem in autonomous vehicles, the limitations of the GPS systems, caused  
52 by GPS outages and the interferences in urban and indoor scenarios, are widely known (because of  
53 buildings, trees, bridges, parking, among others) [18]. For this reason, other approaches focus on  
54 perception solutions for the localization and the environment mapping have been suggested such as:  
55 SLAM, SLAMMOT, among others [19,20]. A survey of the most important algorithms for autonomous  
56 vehicles, based on vision and laser, proposed in the last decade, has been presented in [21]. They claim  
57 that, even if many navigation systems are based on heterogeneous sensors data fusion, the most robust  
58 algorithms are based on visual target tracking, since the position and velocity of the vehicle and the target  
59 relative position can be established by processing the images streams the cameras.

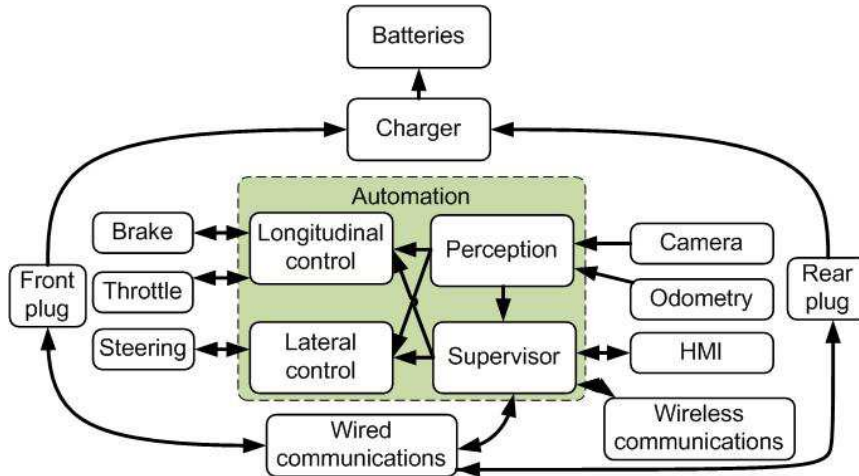
60 Autonomous charging is a well identified issue for electric autonomous systems. This problem has  
61 been historically addressed in robotics [22] and several approaches were proposed based on a wide range  
62 of techniques such as range lights [23] or vision and artificial landmarks [24]. It is really close to the  
63 problem of docking autonomous underwater vehicles (AUVs) for charging purpose [25]. Concerning  
64 autonomous urban vehicles, systems using inductive charging was already proposed [26], but are not  
65 really energy efficient, even if they are easy to handle. Systems that consider docking for charging  
66 electric vehicles require a highly accurate localization and control (a few centimeters), uncommonly  
67 treated in the literature [27,28]. The aim of the research is to design and develop a control system, for  
68 automatic recharging docking for EVs in urban parking areas. The vehicle is equipped with an infrared  
69 camera, able to detect infrared diodes placed on the infrastructure. These diodes are used as landmarks,  
70 in order to provide a highly accurate position and velocity to the control stage. The camera is placed  
71 behind the rear-view mirror (looking ahead), and the vehicle is an electric Citroën C1, instrumented to  
72 enable autonomous driving.

73 This paper is organized as follows: a description of the system architecture and of the AMARE project  
74 objectives are provided in Section 2. The perception algorithms, signal filtering, control stages, followed  
75 by an explanation on the control strategies used in the lateral control law are explained in section 3.  
76 Experimental demonstrations and results obtained with the real facilities are described in section 4. The  
77 paper ends with conclusions and future works in section 5.

## 78 2. System Architecture

79 The automatic docking, recharging, billing and payment system proposed in this paper is composed  
80 of three main elements: an automated vehicle, a docking and recharging station, and a wireless  
81 communication system.

82 Once the vehicle is properly parked by the driver a few meters from the station, the perception system  
83 identifies the infrared LEDs placed in the recharging station, and then the connection procedure is  
84 initiated by the vehicle. The first connection is performed by wireless communications. The vehicle  
85 sends to the station its intention to park and to recharge its batteries. Once accepted by the station, the

**Figure 2.** Automated vehicle on the AMARE project

86 vehicle autonomously docks with the station and the recharging starts without any human intervention  
 87 (Figure 1). When the vehicle intends to leave the station, a billing is calculated given the energy  
 88 consumed by the vehicle and the total parking time. The payment of the charge can be performed  
 89 via a contactless payment system or sent to the driver's billing address for an a posteriori payment.

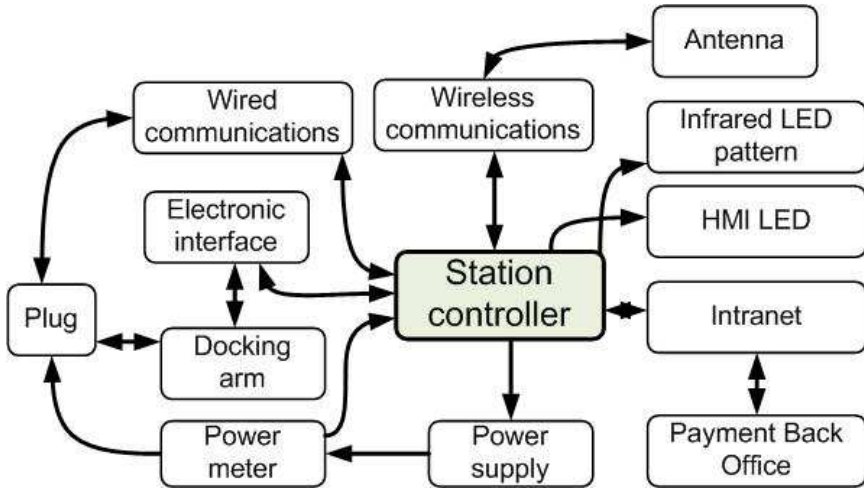
### 90 2.1. Automated Vehicle

91 The vehicle used is an electrified Citroën C1 instrumented for autonomous driving. Figure 2 shows the  
 92 different components used in the autonomous vehicle. The vehicle is equipped with two docking plugs  
 93 - front and back - for battery charging and wired communications. This design allows the connection  
 94 of several vehicles in series to a unique recharging station, reducing the number of recharging stations  
 95 needed. In the meanwhile the physical link between the vehicles can be used to displace all the vehicles  
 96 in a platoon configuration with a unique driver, thus facilitating the redistribution of vehicles between  
 97 stations [29].

98 A wireless communication link is established before the docking procedure with the recharging  
 99 station. The automated vehicle uses the information from the installed infrared camera and the odometry  
 100 to guide the vehicle into its final parking position or docking spot. The perception system (section 3.1)  
 101 starts by estimating the pose of the vehicle relative to the pattern of infrared LEDs in the recharging  
 102 station.

103 The control of the vehicle and driving task is supported by the on-board automation system until  
 104 the vehicle reaches its docking spot. The throttle and brake pedals with integrated potentiometers  
 105 are commanded by the longitudinal controller, and the electric power-assisted steering actuator is  
 106 commanded by the lateral controller (section 3.2).

107 Information about the automatic docking procedures are provided to the driver via the on-board HMI  
 108 (Human Machine Interface) and stored in a remote server. Once the docking is established and the  
 109 vehicle is plugged to the automated arm, a wired connection is established between the vehicle and  
 110 the station. At the same time the recharging of the vehicle batteries starts and the consumed energy is  
 111 registered. This information is used later by the billing process together with the parking time costs.

**Figure 3.** Recharging and docking station on the AMARE project

<sup>112</sup> **2.2. Recharging and Docking Station**

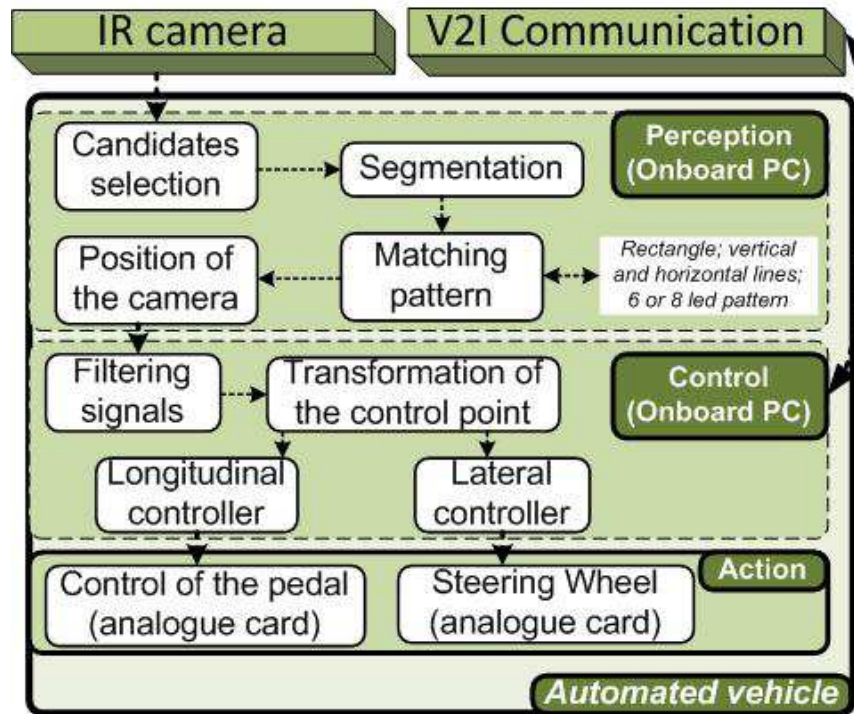
<sup>113</sup> The station, equipped with a docking arm, is used to charge up to five vehicles in series. The  
<sup>114</sup> communication with the vehicles, prior plug-in connection, is done via wireless WiFi communications.  
<sup>115</sup> The station allows/rejects connection requests from the vehicle that want to dock and recharge. The status  
<sup>116</sup> of the station can easily be accessed by the lights interface information (in the station): green - the station  
<sup>117</sup> is available, yellow blinking - the docking arm is being deployed, red - the station is occupied. Once the  
<sup>118</sup> plug is connected to a vehicle, the power supply is activated and the energy consumption is registered  
<sup>119</sup> (figure 3). An infrared LED pattern installed in the station is detected by the vehicle on-board camera  
<sup>120</sup> in order to determine its relative position. The station controller manages the electronic interface that  
<sup>121</sup> controls the docking arm, the power supply and the infrared LED pattern. The controller is connected  
<sup>122</sup> directly to a payment back office through a local network (intranet), and handles the communications  
<sup>123</sup> with the vehicle.

<sup>124</sup> **2.3. Communication System**

<sup>125</sup> The action coordination between the vehicle automation (supervisor) and the station controller  
<sup>126</sup> are performed via an IPv6 wireless link based on embedded Linux boxes (4G Cubes) [8]. This  
<sup>127</sup> communication system is a Vehicle Web Service Communication Framework (VWSCF) that handles  
<sup>128</sup> service discovery, expose and fetch of data through the network. For practical reasons, the payment  
<sup>129</sup> procedure is performed via a different wireless connection using a standard highway contactless payment  
<sup>130</sup> system. Once the vehicle is plugged to the docking arm a wired connection is established and diagnostics  
<sup>131</sup> data are exchanged between the vehicle and the station.

<sup>132</sup> **3. Onboard Algorithms -Autonomous Docking-**

<sup>133</sup> Figure 4 shows the control scheme of the autonomous vehicles docking proposed in this work. It  
<sup>134</sup> considers an infrared camera for the localisation of the vehicle in the reference frame of the charging  
<sup>135</sup> station. After the pattern processing, the relative position is given to the control stage. Then, this position

**Figure 4.** Control architecture for autonomous vehicles based on IR camera information

<sup>136</sup> is filtered and translated to the centre front axis of the vehicle, to improve the control accuracy. Finally,  
<sup>137</sup> a reference command is sent to the action stage. The explanation of each module is described below.

### <sup>138</sup> 3.1. Perception

<sup>139</sup> A standard charge-coupled device (CCD) camera, equipped with an IR filter, was provided by our  
<sup>140</sup> industrial partner in the project and was used in this work, placed behind the rear-view mirror, looking  
<sup>141</sup> front. In our experiment infrared LEDs were used on the docking station instead of visible beacons, to  
<sup>142</sup> simplify their detection from the background and make the system invisible from passers-by.

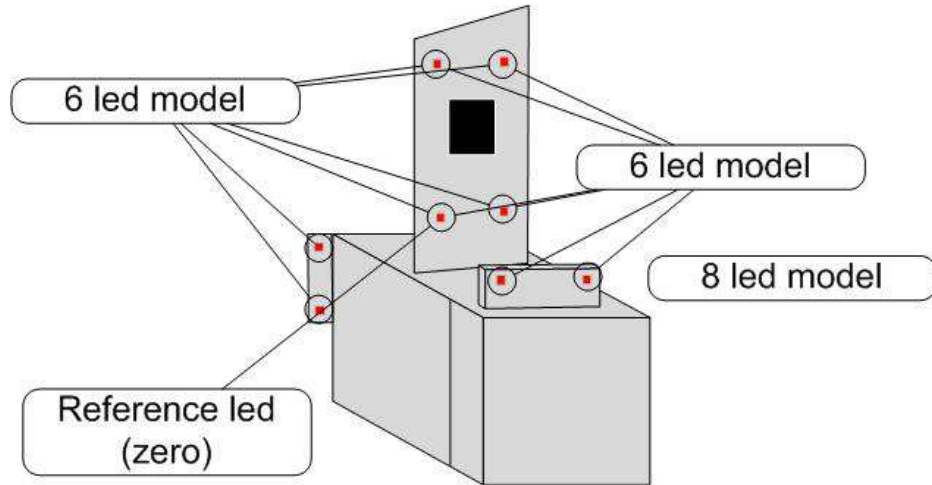
<sup>143</sup> The docking station is equipped with 8 infrared LEDs, their positions being precisely known in  
<sup>144</sup> the station referential. This rather high number of LEDs was chosen to allow the detection of several  
<sup>145</sup> patterns, in case one or several lights were obstructed or failing. Our experiments showed that 6 LEDs  
<sup>146</sup> are enough in practice to accurately determine the vehicle position with regard to its docking station.

<sup>147</sup> Thanks to the camera information, the perception stage computes the position, in Cartesian  
<sup>148</sup> coordinates, and the heading in respect to the reference line, then sends it to the control stage.

#### <sup>149</sup> 3.1.1 Vision Detection Algorithms

<sup>150</sup> This section describes the several steps used in the vision pipeline to get the relative position and the  
<sup>151</sup> informations needed by the control node. From the input picture, the following steps are applied :

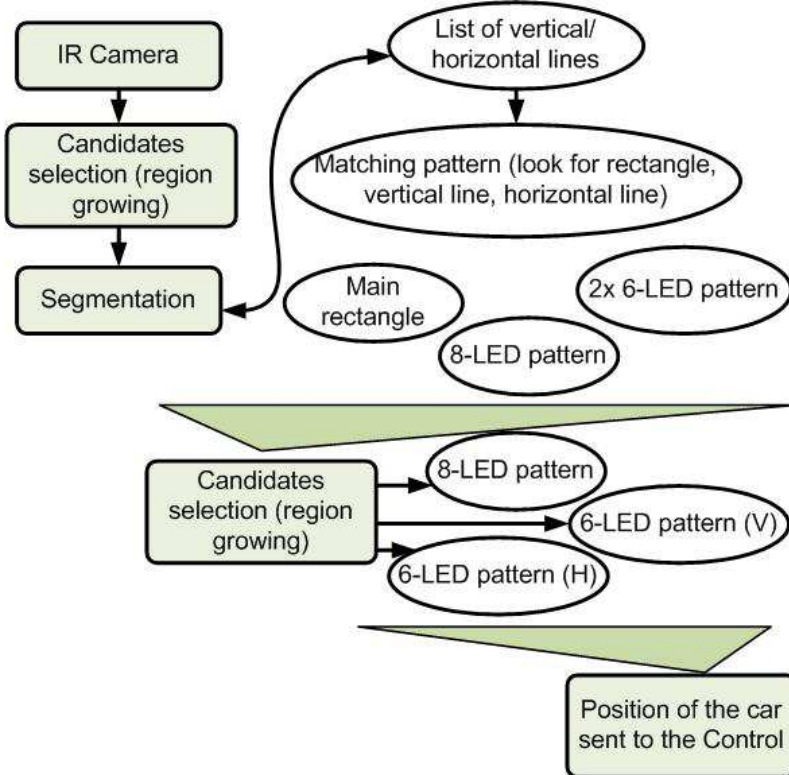
- <sup>152</sup> *1. Maxima selection.* We assume that the LED candidates on the picture are among the brightest  
<sup>153</sup> points, and that they correspond to a local maxima. This is very common for the detection of  
<sup>154</sup> bright features on a picture.

**Figure 5.** Detection algorithms using different models

- 155 2. *Region growing.* From the previously selected extrema, region growing is applied to get the bright  
 156 area. Region-growing halting criteria are based on brightness gradient, and absolute brightness  
 157 level. LEDs models being previously known, a fast model-based selection is used to remove an  
 158 initial set of outliers, *ie* bright areas physically too big to be our LEDs. This rejection effectively  
 159 handles major light sources, such as car lights, sun light or most secular reflections.
- 160 3. *Model fitting.* A list of vertical and horizontal lines stem from the set of LED candidates previously  
 161 detected. Knowing the 3D base model of the station, simple heuristics are used to remove  
 162 candidates leading to improper form-factor. In our case, several constants in LEDs relative position  
 163 (only two LEDs on top) are easy to use to remove trivial mis-fitting candidates. Moreover, this  
 164 step can be simplified for the following detections, a rough initial position for the projected pattern  
 165 being given by previous iteration. Several LED sub-models can be tracked on the station, for an  
 166 extra robustness against occlusions. In our case, three sub-models can be used while keeping the  
 167 POSIT algorithm running (defined by 6 to 8 LEDs), while a rough position can be computed from  
 168 the top 4 LEDs (figure 5).
- 169 4. *POSIT algorithm* (detailed in figure 6). This algorithm, detailed in 3.1.2, provides an estimation of  
 170 the 6D position and attitude as regards the model from its projection into the camera plane. This  
 171 gives a complete determination of the car attitude. POSIT can be run separately on each of the  
 172 four models are detected.

### 173 3.1.2 The POSIT Algorithm

174 This algorithm was first published in [30] by DeMenthon et al., its purpose is to find the pose of an  
 175 object with regard to the camera referential from a single image. This is not a simple task, due to the loss  
 176 of information consecutive to the projection process from the 3D model to the picture plane. Extensive  
 177 pose information typically transfers into six degrees of freedom, degrees which are not necessarily visible  
 178 after the projection onto a 2D plane consecutive to the imaging process. In other words, the projection  
 179 matrix stemming from the standard pinhole camera model is not invertible.

**Figure 6.** Summary of the perception pipeline

180 It is then compulsory to find an estimation of the pose, with an approach robust enough to handle these  
 181 ambiguities gracefully. Several methods were developed over time (see the reference for an extensive  
 182 review), but *POSIT* algorithm is now commonly used for this task, due to its very low coding and  
 183 computing complexity, and its iterative nature. *POSIT* does not require initial pose estimate, and can run  
 184 in real-time on low power hardware.

185 Summing up some of its key ideas, *POSIT* can be split into two steps: pose computation from an  
 186 approximated scaled orthographic projection, and an iteration procedure which allows the algorithm  
 187 to converge without an initial guess. The scaled orthographic projection is close to a perspective  
 188 projection, but differs in that depth coordinates of the model features get the same value in the projection  
 189 computation, thus neglecting intra-object depth differences compared to camera-to-object distance. This  
 190 effectively linearises the projection process. The iteration procedure consists in computing the mismatch  
 191 between the observation ("true" projection of the 3D model onto the image plane) and the computed  
 192 scaled orthographic projection, which gives the pose correction step.

193

194 In practice, *POSIT* converges within 10 iterations, and its reliability can be assessed by computing  
 195 the model features positions onto the image plane from the computed pose, camera pin-hole model and  
 196 the known geometry of the model. A limit of the *POSIT* approximations can however be observed at a  
 197 very close range, when the model depth dimension is not negligible compared to the camera-to-object  
 198 distance.

199 Figure 7 shows a typical view from the perception system. The docking station is correctly identified  
 200 and positioned, as shown by the back projected features of a 6-LED model (white circles) piled onto the  
 201 detected LEDs (end of the white lines). This scene shows a difficult situation, because of a low position

**Figure 7.** Typical view from the system, on the side of a busy road.

of the sun (in front of the camera) and some reflections are detected as a "worst-case scenario". Following the proposed algorithm, an initial region growing algorithm restrained to LEDs reasonable size allows us to create a list of LED candidates, pictured in red squares on Figure 7. The knowledge of the positions of the LED relative to one another is then used to remove improbable LEDs configurations. The recognized configuration is depicted by the white segments in the figure. Finally, the POSIT algorithm can be applied on this recognised projected pattern, in this case on the 6-LEDs sub-model, and the 3D configuration is back-projected on the picture, as shown by the white disks. The correspondence between detected LED positions and 3D projections from the known model and pose is used as a quality check criteria.

### 3.1.3 Filtering

Since the information coming from the camera signal are noisy, a signal filtering is required. To this end, a digital filter implementation in terms based on classical finite impulse response and numerical differentiation is used. This techniques has been developed in the framework of the project ALIEN<sup>1</sup>, which is devoted to study and to develop of new techniques in identification and estimation [31].

The signal coming from the camera is approximated as a truncated Taylor expansion at order  $N$  and for  $t = 0$ .

$$x(t) = \sum_{i \geq 0}^N x^{(i)}(0) \frac{t^i}{i!} \quad (1)$$

Then, each processed signal can be extended in a polynomial function of higher degree and derivative coefficient can be calculated by using the Laplace transform. Here, the  $x(t)$  and  $y(t)$  positions over time are locally represented as a first order polynomial function,  $\forall (a_0, a_1) \in \mathbb{R}^2$ :

$$x(t) = a_0 + a_1 \cdot t \quad (2)$$

<sup>1</sup><http://raweb.inria.fr/rapportsactivite/RA2010/alien/uid1.html>

In order to smooth the signal, coefficient  $a_0$  for  $x(t)$  and  $y(t)$  signals must be estimated. Using the Laplace transform and successive calculus transformation, eq (2) can be expressed in the Laplace domain as:

$$\frac{a_0}{s^2} = 2s \frac{X(s)}{s^2} + \frac{1}{s} \frac{dX(s)}{ds} \quad (3)$$

where  $X(s)$  is the operational expression of  $x(t)$  (and respectively  $Y(s)$  with  $y(t)$ ). Using classical operational to time domain transformation rules and Cauchy formula, estimation of the coefficient  $a_0$  can be limited to one integral:

$$a_0 = \frac{2}{T^2} \int_0^T (2T - 3\delta)x(\delta)d\delta \quad (4)$$

217 where  $T$  is the length of the integration window. More details on this technique are provided in [31–33].

218 **3.2. Control**

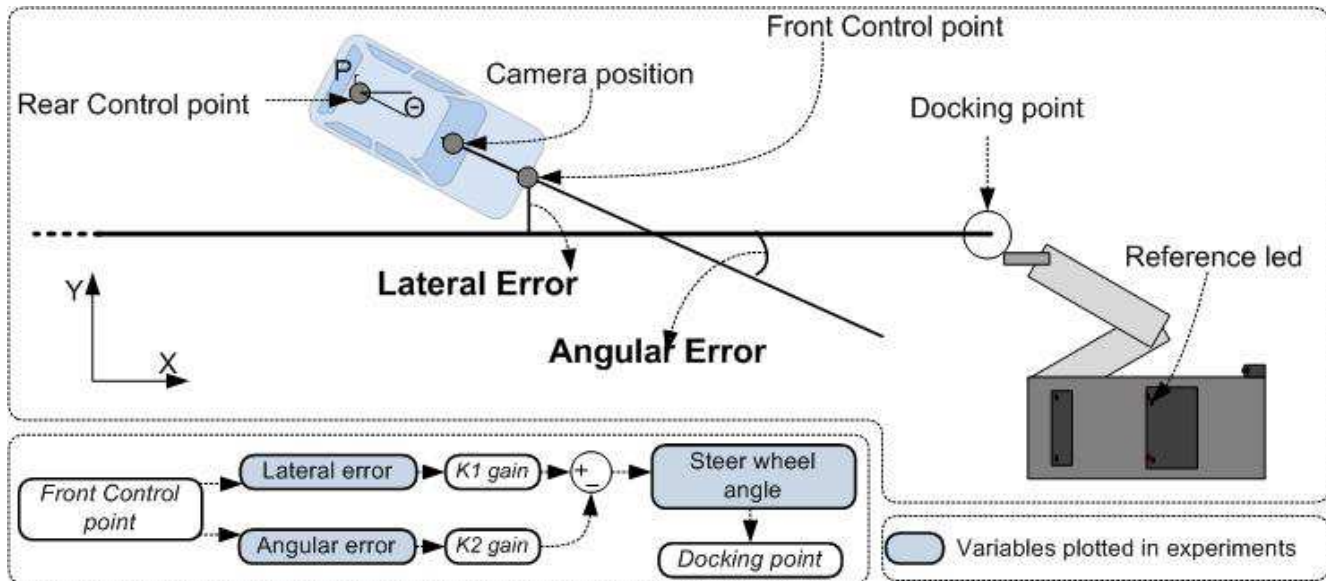
219 Different environments and conditions (speed, data available, among others) determine the control law  
 220 used for autonomous vehicles. Since a real vehicle is a multipart system, some works consider complex  
 221 models or IA techniques to control the vehicle [34,35]. However, under stringent conditions, as low  
 222 constant speed and the absence of dynamic forces (lateral acceleration is zero), simple kinematic model  
 223 can be used. Moreover, it is well accepted in the literature to separate the control in lateral (steering  
 224 wheel) and longitudinal (throttle and brake) for driverless vehicles, both in hardware and software.  
 225 Consequently, each system can run independently.

226 For the longitudinal controller, we used a Proportional Integral (PI) to reach the reference speed, and  
 227 then to reduce the speed when the vehicle is reaching to the docking point. Both controllers, lateral  
 228 and longitudinal, were tested in previous simulations, showing good results [29]. However, in the real  
 229 implementation, only the longitudinal control worked appropriately due to the information coming from  
 230 the camera and that is always available. The bang-bang control law, proposed for the lateral control in  
 231 [29], has been discarded because the maximum vision range of the camera is limited to [-20, 15] degrees  
 232 and there is not odometry integrated in the vehicle. Moreover, in this simulation, the footpath, where  
 233 the charging station is placed, was not considered, therefore the overshoot of this control law can crash  
 234 the front right wheel with the infrastructure. In this section, a new solution for the lateral control in  
 235 autonomous docking for electric vehicles is presented.

236 **3.2.1 Kinematic Model**

237 Due to the low speed of our application, the centrifugal force is considered as despicable, the wheel  
 238 slipping and the forces transferred between wheels of the same axle track are approximated to zero.  
 239 Moreover, the radius of curvature is assumed bigger than the wheel base. Therefore, the kinematic  
 240 model is estimated by the standard bicycle or Ackerman model [36,37], considering that the two front  
 241 wheels turn without different speed, and the rotation center is the medium between them. The differential  
 242 equations, describing the movement in a Cartesian plane ( $x, y$ ), are as follow:

$$\frac{dX}{dt} = V_{(t)} * \cos(\theta) \quad (5)$$

**Figure 8.** Variables used the autonomous docking and the experiments

$$\frac{dY}{dt} = V_{(t)} * \sin(\theta) \quad (6)$$

$$\frac{d\theta}{dt} = \frac{V_{(t)}}{L} * \tan(\alpha) \quad (7)$$

where  $\theta$  is the orientation angle with respect to plane XY,  $\alpha$  is the steering angle of the front wheel,  $L$  is the wheel base, and  $V_{(t)}$  is the longitudinal speed. The point X and Y are defined with respect to the center of the rear axle of the vehicle. Simulation presented in [29] shows good results controlling the rear point (figure 8). However, due to the high precision needed in our application (the vehicle has to reach the docking point with error of  $\pm 5$  cm), it is necessary to translate the control point to the front. The bottom left part of figure 8 shows a block diagram with the input variables used in the control stage, as well as the steering angle output, which reaches the docking point. The next module explains the considerations to this end.

### 3.2.2 Front Control Point

Information coming from the camera provides the position (in Cartesian coordinates) and the angular error from the reference line (in radians) regarding to the camera position (figure 8). The aim of this new module is to calculate the coordinates of the control position from the coordinates of the camera, and also to fit the angle error.

Table 1 shows the properties measured from the docking point to the 'reference LED' to calculate the position (figure 8). The  $AngOffset$  is the balance of the camera with respect to the reference line, since it is slightly turned to capture more LEDs in the right side of the vehicle. The  $Dist_{target}$  is the distance from the camera (in the rear-view mirror) to the nose of the vehicle (where the front control point is placed). The  $X_{offset}$  and  $Y_{offset}$  are offset distances from the reference LED to the docking point (figure 8).

**Table 1.** Parameters to calculate the front control point

Parameters	Values
$Dist_{target}$	1.17 meters
$X_{offset}$	1 meter
$Y_{offset}$	1.36 meters
$AngOffset$	2.3 degrees

262 The new control points, and the angular error are calculated as follow:

$$Angle_{new} = Angle_{camera} - \frac{AngOffset * \pi}{180} \quad (8)$$

$$X_{front} = X_{camera} - \cos(Angle_{new}) * Dist_{target} - X_{offset} \quad (9)$$

$$Y_{front} = Y_{camera} + \sin(Angle_{new}) * Dist_{target} - Y_{offset} \quad (10)$$

### 263 3.2.3 Lateral Control

264 Two control variables that were used for the lateral control law are the lateral and angular errors, as  
 265 proposed in previous works [37,38]. Both errors are calculated in the front control point (in meters) and  
 266 reference line (in degrees) respectively.  $K_1$  and  $K_2$  are the gains fixed manually on the vehicle. The  
 267 first has a proportional effect in control action, since it is associated to error in  $Y$ . Otherwise,  $K_2$  has a  
 268 derivative influence in the control behavior  $\frac{dY}{dt}$ . From equation 6 two facts can assumed: the speed is  
 269 constant in our experiments and the orientation angle ( $\theta$ ) is small (constraints of the camera information).  
 270 Then, equation 6 can be rewritten as follows:

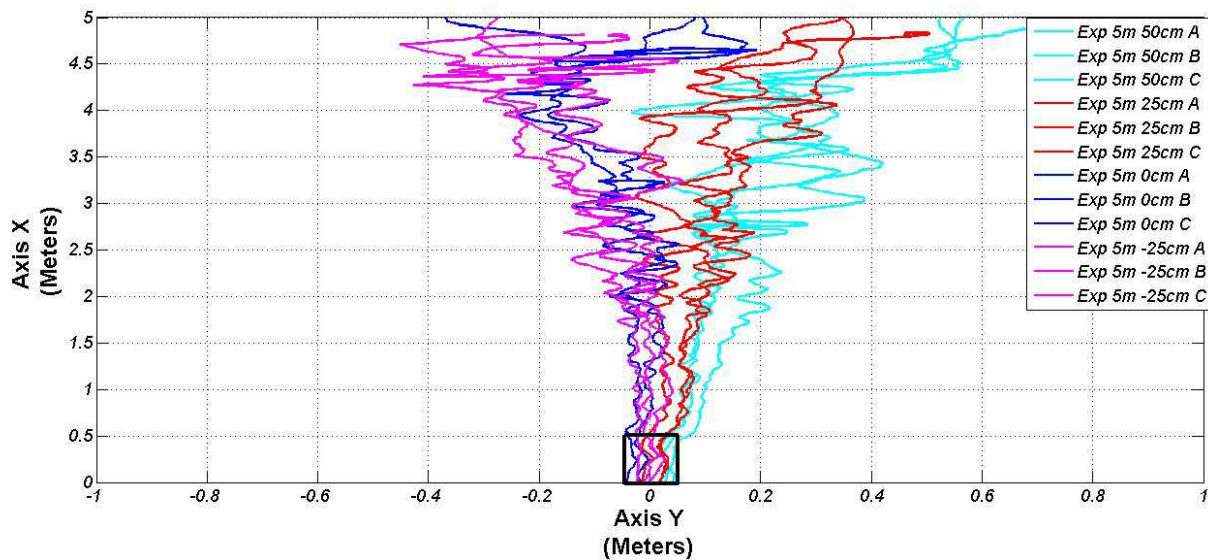
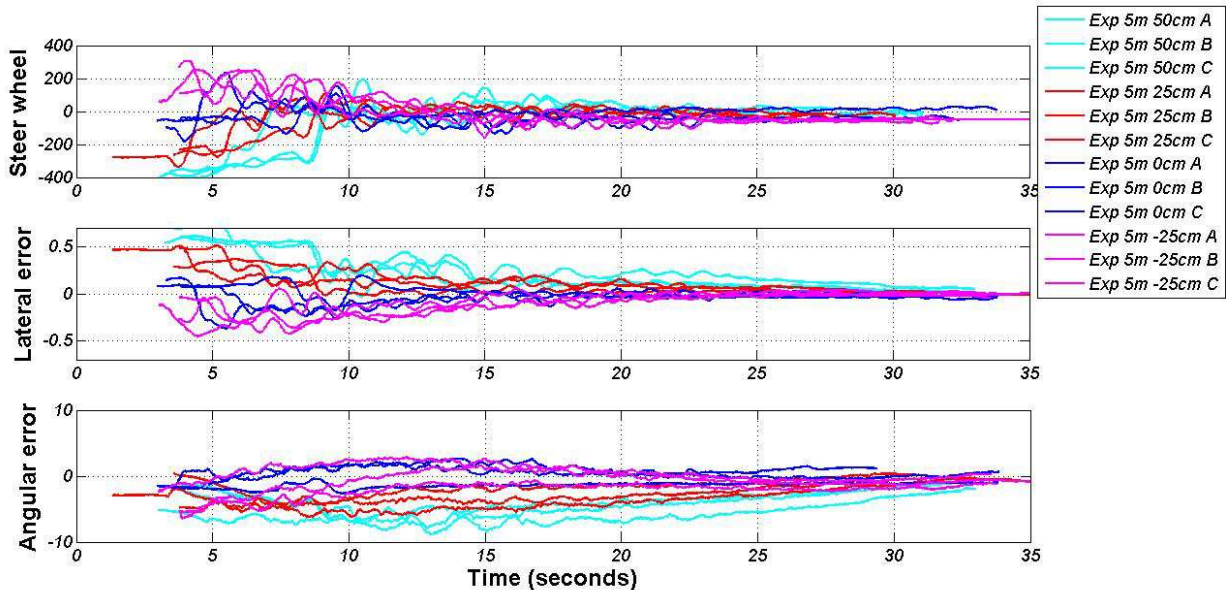
$$\frac{dY}{dt} = V * \theta \quad (11)$$

271 where  $\theta$  is proportional to  $\frac{dY}{dt}$  (angular error). Therefore,  $K_2$  has a derivative action in our system.  
 272 According to the control systems controlled by a PD,  $K_1$  reduces the lateral error (meters) and  $K_2$  helps  
 273 to avoid oscillations and allows a faster and softer output. The final values used -not normalize steering  
 274 wheel output- are 700 and 45 respectively. Finally, an explicit form of the control law used, showing the  
 275 proportional and derivative terms -according to the reference line ( $Lat_{error}$ )- is rewritten as follows:

$$U_{(t)} = K_1 * Lat_{error} - K_2/V * \frac{dLat_{error}}{dt} \quad (12)$$

## 276 4. Results and Discussion

277 After the authentication of the perception system, a validation of the entire system implemented in  
 278 our electric vehicle is described (Figure 1). They illustrate the performance from different X and Y  
 279 starting points (from 3 to 5 meter, and 0 to 50 centimeters, respectively). Due to the footpath, the  
 280 negative values of Y axes are not considered for real implementation. However, one experiment has

**Figure 9.** Validation tests -positioning-**Figure 10.** Validation tests -input variables and action lateral controller-

281 completed from -25 centimeters to validate our control architecture. All the experiments performance  
 282 in the subsection were carried out in the INRIA facilities with the same vehicle, charging station and  
 283 perception system described in section 2.1. Figure 9 shows four different validation tests. Every  
 284 experiment was executed three times around the same starting reference. This figure shows the position  
 285 in Cartesian coordinates, coming from the front control point module, described in section 3.2.2. In the  
 286 lower middle part of the same figure, a reference square shows that the vehicle arrives with a small error  
 287 to the docking point ( $\leq \pm 5$  cm).

288 The upper picture in figure 10 shows the steering wheel control output according to each experiment.  
 289 The light blue graphic (departure point 5 meters and 50 cm for X and Y axes, respectively) shows that  
 290 the steering wheel is turning around -400 degrees, and then softly it returns to the center. The trajectory

**Table 2.** Departure and arrival points in different situations

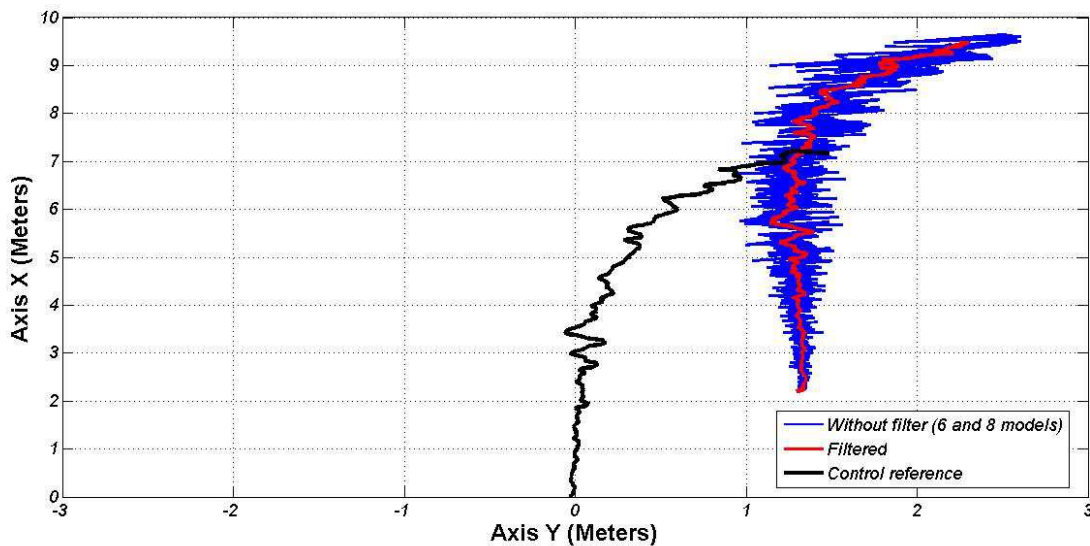
Experiments	Actual Positions and yaw					
	Departure			Arrival		
	$X_{mm}$	$Y_{mm}$	$Yaw$	$X_{mm}$	$Y_{mm}$	$Yaw$
X=5m and Y=50cm	4988.6	481.4	-2.8	27.1	26.0	-3.2
	4963.7	479.2	0.6	37.0	-8.2	-2.1
	4980.4	442.1	4.9	31.5	-2.9	-2.0
X=5m and Y=25cm	5010.5	308.9	-0.2	17.5	-5.1	-1.8
	5011.6	299.3	2.8	33.7	6.7	-1.1
	4996.7	250.2	-1.8	40.0	-3.9	-1.9
X=5m and Y=0cm	5018.9	-14.5	1.4	20.8	14.5	-0.6
	5002.2	-125.2	1.1	-25.8	16.2	-0.2
	5004.0	-24.1	2.2	37.1	28.9	1.1
X=5m and Y=-25cm	5022.0	-251.4	1.3	24.0	32.9	0.7
	5012.9	-202.7	-2.7	17.1	21.3	-0.1
	5015.5	-260.8	-0.9	23.4	25.3	0.3
X=3m and Y=25cm	3026.4	191.7	0.6	40.0	-1.0	-1.4
	3041.8	261.1	1.1	24.5	9.4	-2.2
	3122.5	260.7	-1.1	22.8	-15.9	-2.6

is continuous and without overshoot due to the filtering of the input variables (section 3.1.3). The middle and the lower pictures show the evolution of both input variables: the lateral and angular error. Both have a tendency to zero, and the error in both lateral and angular (yaw) are small (table 2), creating a good docking between vehicle and infrastructure charging arm. The lateral error has been measured with an external distance measure laser in order to have real values concerning to the distance between the vehicle and the docking point.

Table 2 shows the departure and arrival points in every experiment in millimeters, as well as the yaw of the vehicle. Both lateral and longitudinal controllers have reached the minimal error permitted in our application. The averages of the lateral and longitudinal errors, considering the set of experiments are 24.7 and 9.61 millimeters, respectively. Both errors are low, and the vehicle docks inside the valid range ( $\leq \pm 50$  mm). Moreover, the arrival yaw is also low (the root mean square error is 1.05 degrees). It is important in order to have a better docking in the charging station.

Finally, an experiment from a greater distance, both in X and Y axes (7.5 and 1.25 meters, respectively), have been performed. Figure 11 shows the position in Cartesian coordinates from the perception system, filtered and translated to the front control point. As in the previous experiments, the vehicle reaches the docking point with error lower than 5cm.

Figure 12 shows the evolution of the steering position and both input variables. The control action is soft and continuous, and the vehicle never overpasses the reference line (zero in the Y axis). Around 20 s of the experiment, the vehicle arrived to center of the docking line, but it is not completely straight, then the angular action turn the steering wheel until (35 s) the vehicle reaches the docking point with a lateral

**Figure 11.** Positions gave from the perception system in the final experiment

311 and angular error of 2 cm and 0.4 degrees, respectively. Then, the automatic charging arm is ready to  
 312 charge the batteries.

## 313 5. Conclusions and Future Works

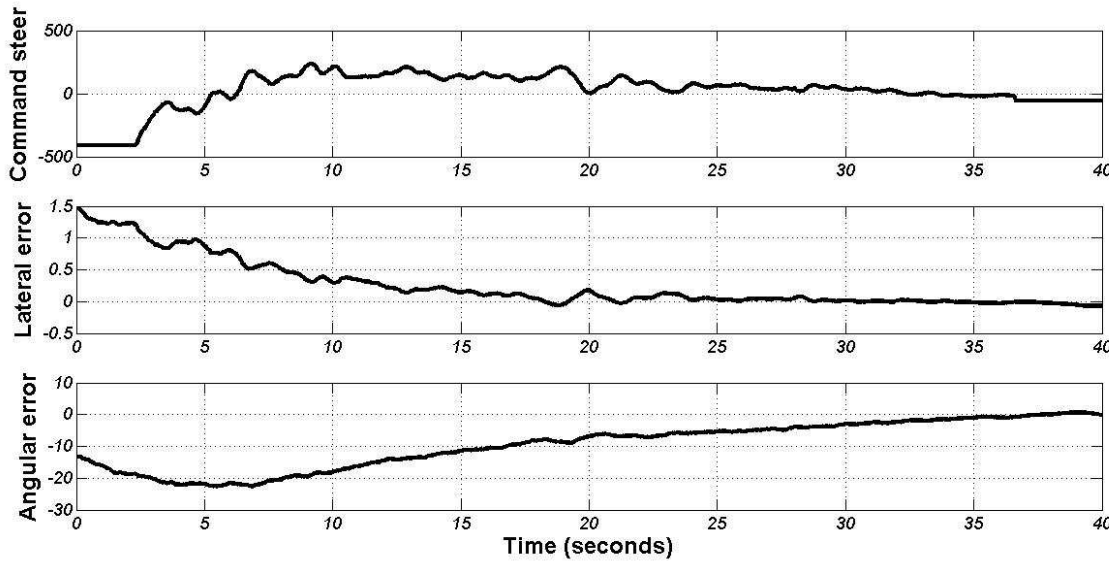
314 In this work, control architecture for autonomous docking systems, based on an embedded perception  
 315 system in an autonomous electric vehicle and a recharging station for urban parking areas is presented.  
 316 Our approach has been developed under the framework of the AMARE project, using the information  
 317 provided by an infrared camera and diodes installed in the recharging station. The information from this  
 318 sensor had been processed and filtered, and then sent to the control stage, for the automatic docking of  
 319 the vehicle. The proposed architecture is easily adaptable to any commercial electric vehicle.

320 Different experiments, departing from different points, show a good behaviour of the proposed  
 321 system. Both lateral and longitudinal errors are lower than the limits of the charging station. The proposed  
 322 controller is easy and intuitive for tuning, and the gains can be adapted according to the different vehicles  
 323 characteristics. This technology assists to human drivers in the charging and docking process of electric  
 324 vehicles in cities.

325 The system presented in this paper is actually working in a real scenario on the city of Paris <sup>2</sup> as a  
 326 permanent demonstrator of the AMARE project.

327 The proposed work relies solely on the information from the camera on board the vehicle. When the  
 328 charging station is out-of-range, the camera is obstructed, the signal is too noisy or is lost(v.g. if the  
 329 steering wheel turns a lot), the autonomous docking manoeuvre is stopped until the signal is perceived  
 330 again. For this reason, other sensors and data information may be added to the control architecture  
 331 proposed, such as: CAN frame data or odometer data, in order to increase the redundancy and the  
 332 robustness of the system in future works. Moreover, actions over the gear shift can be considered for  
 333 more constrained scenarios.

<sup>2</sup>[http://www.modulowatt.com/Modulowatt\\_video\\_Mobilier\\_Urbain\\_Intelligent\\_fr.html](http://www.modulowatt.com/Modulowatt_video_Mobilier_Urbain_Intelligent_fr.html)

**Figure 12.** Lateral command and variables of the control in the last experiment

### 334 Acknowledgements

335 This work was supported by the projet Amare, financed by ADEME (*Agence de l'Environnement et*  
 336 *de la Maîtrise de l'Energie*)

### 337 References

- 338 1. Lin, B.F.; Chan, Y.M.; Fu, L.C.; Hsiao, P.Y.; Chuang, L.A.; Huang, S.S. Incorporating  
 339 appearance and edge features for vehicle detection in the blind-spot area. *Proc. 13th Int*  
 340 *Intelligent Transportation Systems (ITSC) IEEE Conf*, 2010, pp. 869–874.
- 341 2. Bansal, M.; Das, A.; Kreutzer, G.; Eledath, J.; Kumar, R.; Sawhney, H. Vision-based Perception  
 342 for Autonomous Urban Navigation. *IEEE International Conference on Intelligent Transportation*  
 343 *Systems (ITSC)*, 2008, pp. 434–440.
- 344 3. Puthon, A.S.; Nashashibi, F.; Bradai, B. A complete system to determine the speed limit by  
 345 fusing a GIS and a camera **2011**. pp. 1686–1691. ANR.
- 346 4. Llorca, D.F.; Milanés, V.; Alonso, I.P.; Gavilán, M.; Daza, I.G.; Pérez, J.; Sotelo, M.A.  
 347 Autonomous Pedestrian Collision Avoidance Using a Fuzzy Steering Controller. *IEEE*  
 348 *Transactions on Intelligent Transportation Systems* **2011**, *12*, 390–401.
- 349 5. Paromtchik, I.; Laugier, C. Motion generation and control for parking an autonomous vehicle.  
 350 *IEEE International Conference on Robotics and Automation (ICRA)*, 1996, Vol. 4, pp. 3117  
 351 –3122 vol.4.
- 352 6. Final Report: Study on Clean Transport Systems. Technical report, European Commission,  
 353 Directorate-General for Mobility and Transport, 2011.
- 354 7. Xia, T.; Yang, M.; Yang, R.; Wang, C. CyberC3: A Prototype Cybernetic Transportation System  
 355 for Urban Applications. *IEEE Transactions on Intelligent Transportation Systems* **2011**, *11*, 142–  
 356 152.

- 357 8. Bouraoui, L.; Boussard, C.; Charlot, F.; Holguin, C.; Nashashibi, F.; Parent, M.; Resende, P. An  
358 on-demand personal automated transport system: The CityMobil demonstration in La Rochelle.  
359 IEEE Intelligent Vehicles Symposium (IV), 2011, pp. 1086–1091.
- 360 9. Harris, A. Charge of the electric car - [power electric vehicles]. *Engineering Technology* **2009**,  
361 4, 52–53.
- 362 10. Budhia, M.; Covic, G.; Boys, J. A new IPT magnetic coupler for electric vehicle charging  
363 systems. 36th Annual Conference on IEEE Industrial Electronics Society (IECON), 2010, pp.  
364 2487–2492.
- 365 11. Etezadi-Amoli, M.; Choma, K.; Stefani, J. Rapid-Charge Electric-Vehicle Stations. *IEEE*  
366 *Transactions on Power Delivery* **2010**, 25, 1883–1887.
- 367 12. Naranjo, J.; Bouraoui, L.; Garcia, R.; Parent, M.; Sotelo, M. Interoperable Control Architecture  
368 for Cyberscars and Dual-Mode Cars. *IEEE Transactions on Intelligent Transportation Systems*  
369 **2009**, 10, 146–154.
- 370 13. Bouraoui, L.; Petti, S.; Laouiti, A.; Fraichard, T.; Parent, M. Cybercar Cooperation for Safe  
371 Intersections. IEEE International Conference on Intelligent Transportation Systems Conference  
372 (ITSC), 2006, pp. 456–461.
- 373 14. Moriwaki, K. Mathematical modeling and control of an autonomous electric vehicle for  
374 navigation and guidance. IEEE International Electric Vehicle Conference (IEVC), 2012, pp.  
375 1–8.
- 376 15. Yih, P.; Gerdes, J.C. Modification of vehicle handling characteristics via steer-by-wire **2005**.  
377 13, 965–976.
- 378 16. Pérez, J.; Gajate, A.; Milanes, V.; Onieva, E.; Santos, M. Design and Implementation of a  
379 Neuro-Fuzzy System for Longitudinal Control of Autonomous Vehicles. Proc. IEEE World  
380 Congress on Computational Intelligence WCCI 2010, 2010, pp. 1–5.
- 381 17. Milanés, V.; Naranjo, J.; Gonzalez, C.; Alonso, J.; de Pedro, T. Autonomous vehicle based in  
382 cooperative GPS and inertial systems. *Robotica* **2008**, 26, 627–633.
- 383 18. Mao, X.; Wada, M.; Hashimoto, H. Nonlinear GPS models for position estimate using low-cost  
384 GPS receiver. Proceedings Intelligent Transportation Systems Conference (ITSC), 2003, Vol. 1,  
385 pp. 637–642 vol.1.
- 386 19. Xie, J.; Nashashibi, F.; Parent, M.; Favrot, O. A real-time robust global localization for  
387 autonomous mobile robots in large environments. 11th International Conference on Control  
388 Automation Robotics Vision (ICARCV), 2010, pp. 1397–1402.
- 389 20. Zhang, X.; Rad, A.; Wong, Y. Sensor Fusion of Monocular Cameras and Laser Rangefinders  
390 for Line-Based Simultaneous Localization and Mapping (SLAM) Tasks in Autonomous Mobile  
391 Robots. *Sensors* **2012**, 12(1), 429–452.
- 392 21. Jia, Z.; Balasuriya, A.; Challa, S. Autonomous Vehicles Navigation with Visual Target Tracking:  
393 Technical Approaches. *Sensors* **2008**, 1(2), 153–182.
- 394 22. Silverman, M.; Nies, D.; Jung, B.; Sukhatme, G. Staying alive: a docking station for autonomous  
395 robot recharging. IEEE International Conference on Robotics and Automation (ICRA), 2002,  
396 Vol. 1, pp. 1050–1055 vol.1.

- 397 23. Cassinis, R.; Tampalini, F.; Bartolini, P.; Fedrigotti, R. Docking and charging system for  
398 autonomous mobile robots. *Department of Electronics for Automation, University of Brescia,  
399 Italy* **2005**.
- 400 24. Luo, R.; Liao, C.; Su, K.; Lin, K. Automatic docking and recharging system for autonomous  
401 security robot. IEEE/RSJ International Conference on Intelligent Robots and Systems (IROS),  
402 2005, pp. 2953 – 2958.
- 403 25. Singh, H.; Bellingham, J.; Hover, F.; Lemer, S.; Moran, B.; von der Heydt, K.; Yoerger, D.  
404 Docking for an autonomous ocean sampling network. *IEEE Journal of Oceanic Engineering*  
405 **2001**, *26*, 498 –514.
- 406 26. Bleijs, C.; Normand, O. A fully automatic station using inductive charging techniques. Proc. of  
407 the Thirteenth Int. Symp. on Electric Vehicle, Osaka, J, 1996.
- 408 27. Wong, J.; Nejat, G.; Fenton, R.; Benhabib, B. A neural-network approach to high-precision  
409 docking of autonomous vehicles/platforms. *Robotica* **2007**, *25*, 479–492.
- 410 28. Martin, J. Design for implementation: fully integrated charging & docking infrastructure used in  
411 Mobility-on-Demand electric vehicle fleets. PhD thesis, Massachusetts Institute of Technology,  
412 2012.
- 413 29. Petrov, P.; Boussard, C.; Ammoun, S.; Nashashibi, F. A hybrid control for automatic docking  
414 of electric vehicles for recharging. IEEE International Conference on Robotics and Automation  
415 (ICRA), 2012, pp. 2966 –2971.
- 416 30. DeMenthon, D.F.; Davis, L.S. Model-based object pose in 25 lines of code. *International Journal  
417 of Computer Vision* **1995**, *15*, 123–141.
- 418 31. Fliess, M.; Join, C.; Sira-Ramirez, H. Non-linear estimation is easy. *Int. J. Modelling  
419 Identification and Control* **2008**, *4*, 12–27.
- 420 32. Fliess, M.; Sira-Ramírez, H. An algebraic framework for linear identification. *ESAIM: Control,  
421 Optimisation and Calculus of Variations* **2003**, *9*, 151–168.
- 422 33. Mboup, M.; Join, C.; Fliess, M. Numerical differentiation with annihilators in noisy environment.  
423 *Numerical Algorithms* **2009**, *50*, 439–467. 10.1007/s11075-008-9236-1.
- 424 34. Villagrá, J.; Milanés, V.; Pérez, J.; Godoy, J. Smooth path and speed planning for an automated  
425 public transport vehicle. *Robotics and Autonomous Systems* **2012**, *60* (2), 252–265.
- 426 35. Pérez, J.; Milanés, V.; Onieva, E. Cascade Architecture for Lateral Control in Autonomous  
427 Vehicles. *IEEE Transactions on Intelligent Transportation Systems* **2011**, *12*, 73–82.
- 428 36. Ackermann, T.B.J.; Bünte, T.; Odenthal, D. Advantages of Active Steering for Vehicle Dynamics  
429 Control. *German Aerospace Center* **1999**, *99ME013*.
- 430 37. Sotelo, M.A. Lateral control strategy for autonomous steering of Ackerman-like vehicles.  
431 *Robotics and Autonomous Systems* **2003**, *45*, 223–233.
- 432 38. Pérez, J.; Milanes, V.; de Pedro, T.; Vlacic, L. Autonomous driving manoeuvres in urban road  
433 traffic environment: a study on roundabouts. 18th World Congress of the International Federation  
434 of Automatic Control (IFAC), 2011, pp. 1–5.

435 © January 23, 2013 by the authors; submitted to *Sensors* for possible open access  
436 publication under the terms and conditions of the Creative Commons Attribution license  
437 <http://creativecommons.org/licenses/by/3.0/>.